

Title: Seismic Reliability Assessment of Mid- and High-rise Post-tensioned CLT Shear Wall Structures

Authors: Xiaofeng Sun, Tongji University
Zheng Li, Tongji University
Minjuan He, Tongji University

Subjects: Civil Engineering
Construction
Seismic

Keywords: Cross-Laminated Timber
Post-Tensioned
Seismic
Shear Wall
Structure

Publication Date: 2020

Original Publication: International Journal of High-Rise Buildings Volume 9 Number 2

Paper Type:

1. Book chapter/Part chapter
2. **Journal paper**
3. Conference proceeding
4. Unpublished conference paper
5. Magazine article
6. Unpublished

Seismic Reliability Assessment of Mid- and High-rise Post-tensioned CLT Shear Wall Structures

Xiaofeng Sun, Zheng Li, and Minjuan He[†]

Department of Structural Engineering, Tongji University, Shanghai, 200092, China

Abstract

Currently, few studies have been conducted to comprehend the seismic reliability of post-tensioned (PT) CLT shear wall structures, due to the complexity of this kind of structural system as well as due to lack of a reliable structural model. In this paper, a set of 4-, 8-, 12-, and 16-storey benchmark PT CLT shear wall structures (PT-CLTstrs) were designed using the direct displacement-based design method, and their calibrated structural models were developed. The seismic reliability of each PT-CLTstr was assessed based on the fragility analysis and based on the response surface method (RSM), respectively. The fragility-based reliability index and the RSM-based reliability index were then compared, for each PT-CLTstr and for each seismic hazard level. Results show that the RSM-based reliabilities are slightly less than the fragility-based reliabilities. Overall, both the RSM and the fragility-based reliability method can be used as efficient approaches for assessing the seismic reliabilities of the PT-CLTstrs. For these studied mid- and high-rise benchmark PT-CLTstrs, following their fragility-based reliabilities, the 8-storey PT-CLTstr is subjected to the least seismic vulnerability; while, following their RSM-based reliabilities, the 4-storey PT-CLTstr is subjected to the least seismic vulnerability.

Keywords: Cross-laminated timber, post-tensioned timber structure, seismic reliability, fragility analysis, response surface method.

1. Introduction

Cross-laminated timber (CLT) is suitable for shear wall applications in mid- and high-rise timber structures, due to its positive characteristics including high in-plane shear strength, ideal integrity, good thermal insulation performance, etc. A series of tests were conducted on CLT shear walls (Gavric *et al.* 2015; Pai *et al.* 2017; Deng *et al.* 2019; Shahnewaz *et al.* 2019) and on CLT structural systems (Ceccotti *et al.* 2013; Gavric *et al.* 2015; Porcu *et al.* 2018; van de Lindt *et al.* 2019), in which the CLT wall panels were connected to the foundation or the floor diaphragm using metal connections (e.g., hold-downs and angle brackets). It was attested that the CLT shear walls were always deforming as rigid bodies in the tests, and the areas of the metal connections were prone to premature damages. For overcoming this damage mode commonly occurring in the CLT shear walls and for enhancing their lateral performance, the concept of self-centering massive timber (i.e., CLT or laminated veneer lumber (LVL)) shear walls was proposed (Palermo *et al.* 2006; Smith *et al.* 2007). In these massive timber shear walls, post-tensioning strands or bars were incorporated in the wall panels for providing the self-centering force, therefore, forming the post-tensioned (PT) CLT or LVL shear walls. Sometimes, energy dissipaters (e.g., mild steel dissipater and friction

dissipater) were mounted in the PT massive timber shear walls, for increasing their ductility and energy-dissipating abilities. Such a hybrid massive timber system combining the post-tensioning strands or bars and the energy dissipaters has attracted the interests from the fields of both engineering and scientific research. For the PT LVL shear walls, Buchanan *et al.* (2007) tested the lateral performance of coupled PT LVL shear walls with steel dissipaters; Newcombe *et al.* (2010) tested the lateral performance of one two-thirds-scale two-storey PT LVL shear wall structure. For both the dissipative PT LVL shear wall and the PT LVL shear wall structure, a good self-centering performance with ideal energy-dissipating abilities under seismic loads was attested. Furthermore, Sarti *et al.* (2015; 2017) investigated the seismic design factors for the PT LVL shear wall structures based on both experimental and analytical researches.

Currently, the concept of this hybrid massive timber system has been extended to the field of CLT shear walls. A series of studies have focused on the lateral performance of PT CLT shear walls and on the seismic performance of PT CLT shear wall structures (PT-CLTstrs). Ganey *et al.* (2017) tested the lateral performance of the PT CLT shear walls with or without dissipaters; following Ganey's work, Akbas *et al.* (2017) developed the shear wall model and defined several typical limit states for the PT CLT shear walls. Wilson *et al.* (2019) developed one elastic-plastic predictive model for PT CLT shear walls using the 8-node solid elements. Chen *et al.* (2020) tested

[†]Corresponding author: Minjuan He
E-mail: hemj@tongji.edu.cn

full-scale PT-CLT shear walls with four configurations amounted with the axial energy dissipaters. It was observed that localized crushing of wood occurred in the CLT wall toe, when the drift reached or exceeded 2.5%. As for the structural seismic performance, Pei *et al.* (2019) and Blomgren *et al.* (2019) studied the dynamic performance of one full-scale 2-story building that utilized a lateral load-resisting system consisting of two PT-CLT shear walls. It was attested that the structural system could remain stable self-centering performance even in case of a roof drift pushed to 5%; besides, this structural system can satisfy the life-safety requirement in maximum considered earthquakes (MCEs). Sun *et al.* (2019; 2020a; 2020b; 2020c) tested the lateral performance of 0.5-scale two-storey PT CLT shear walls constructed by the platform method, and then analyzed the seismic response of the PT-CLTstrs with or without dissipaters. For the immediate occupancy (IO), life safety (LS), and collapse prevention (CP) hazard levels, the structural drift limitations were recommended as 0.7%, 1.4%, and 2.2%, respectively.

The structural seismic performance can be quantified using probabilistic methods that combine reasonable performance-based criteria; therefore, several researchers have focused on the seismic reliability analysis on different types of timber structures. van de Lindt and Walz (2003) analyzed the seismic reliability of light-frame wood shear walls based on a developed model for dynamic performance. Li *et al.* (2012) investigated the seismic reliability of post-and-beam timber buildings, considering the uncertainties from earthquakes, structural mass and shear wall characteristics. Zhang *et al.* (2018) assessed the seismic reliability of timber-steel hybrid system and found that the earthquake ground motion was the most significant factor for the

structural seismic reliability. Hong and Yang (2019) estimated the seismic reliability for mid- and high-rise wood buildings constructed with glulam for beams or columns, and with CLT for shear walls or floor diaphragms. Stellacci *et al.* (2018) assessed the currently adopted rehabilitation techniques for traditional timber frame walls by analyzing their structural reliabilities. However, currently few studies have been conducted to comprehend the seismic reliability of PT-CLTstrs, due to the complexity of this kind of structural system as well as due to lack of a reliable structural model.

In this paper, for considering the effect of total floor number, a set of 4-, 8-, 12-, and 16-storey PT CLT shear wall structures (PT-CLTstrs) were designed using the direct displacement-based design (DDD) method. The model of each PT-CLTstr was developed and calibrated. The seismic reliability of each PT-CLTstr was assessed based on the fragility analysis and based on the response surface method (RSM), respectively. The fragility-based reliability index and the RSM-based reliability index were obtained and then compared, for each PT-CLTstr and for each seismic hazard level (i.e., IO, LS, and CP hazard level). The study can provide a technical basis for the PT-CLTstrs in terms of the seismic performance quantification and the floor number optimization.

2. Structural Model Calibration

Three 0.5-scale two-storey PT CLT shear walls with different initial post-tensioning stress ratios were tested; besides, their numerical models that could accurately predict the lateral performance were also developed, as shown in Figure 1. The floor diaphragm incorporated in

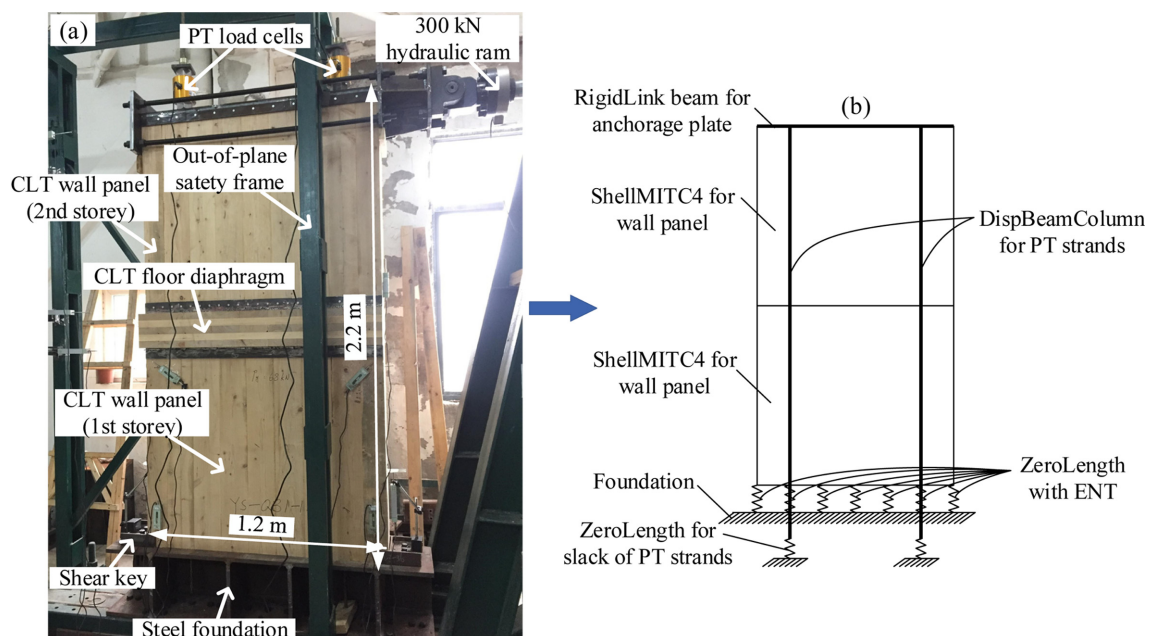


Figure 1. Post-tensioned CLT Shear Wall: (a) Test setup; (b) Model (Sun *et al.* 2020a)

the shear wall specimen was structurally designed for mitigating its creep deformation under the perpendicular-to-grain compression. More details of the shear wall specimens and of the predictive shear wall model are introduced by Sun *et al.* (2019; 2020a). The CLT for the shear wall specimens was fabricated with No.2-grade Canadian hemlock. He *et al.* (2018) tested the mechanical properties of this Canadian hemlock CLT, and found that the CLT can provide ideal compressive or bending properties for engineering applications. Then, 4-, 8-, 12-, and 16-storey benchmark PT-CLTstrs (Figure 2) were respectively designed using the DDD method, which was proven to be suitable for designing the PT-CLTstrs with or without the dissipaters (Sun *et al.* 2019). The storey height of the PT-CLTstrs (H) was designed as 2600 mm. For the DDD-based PT-CLTstrs with dissipaters and those without dissipaters, their response of inter-storey drift was similar under identical seismic hazard level (Sun *et al.* 2019 and 2020c). Since the inter-storey drift was used

as the measurement of the structural seismic damages, therefore, for increasing the efficiency of numerical calculation, it was determined that no dissipaters were amounted in the designed benchmark PT-CLTstrs. These benchmark PT-CLTstrs designed with the wall panels of every two floors being post-tensioned into one single rocking segment were assumed located in Sichuan, China; the floor weight and the roof weight was respectively obtained as 2.466×10^5 kg and 2.041×10^5 kg based on the gravity analysis. The detailed DDD procedure for the PT-CLTstrs was described by Sun *et al.* (2020c). A summary of the shear wall Y-direction layout for the 4-storey PT-CLTstr is listed in Table 1 as an example; the shear wall layouts of the 8-, 12-, and 16-storey PT-CLTstrs were provided by Sun *et al.* (2019). Based on the design results of the shear wall layout for each PT-CLTstr, the simplified two-dimensional structural model was developed using OpenSees, as shown in Figure 3. The fiber-based DispBeamColumn element was used for simulating the post-tensioning

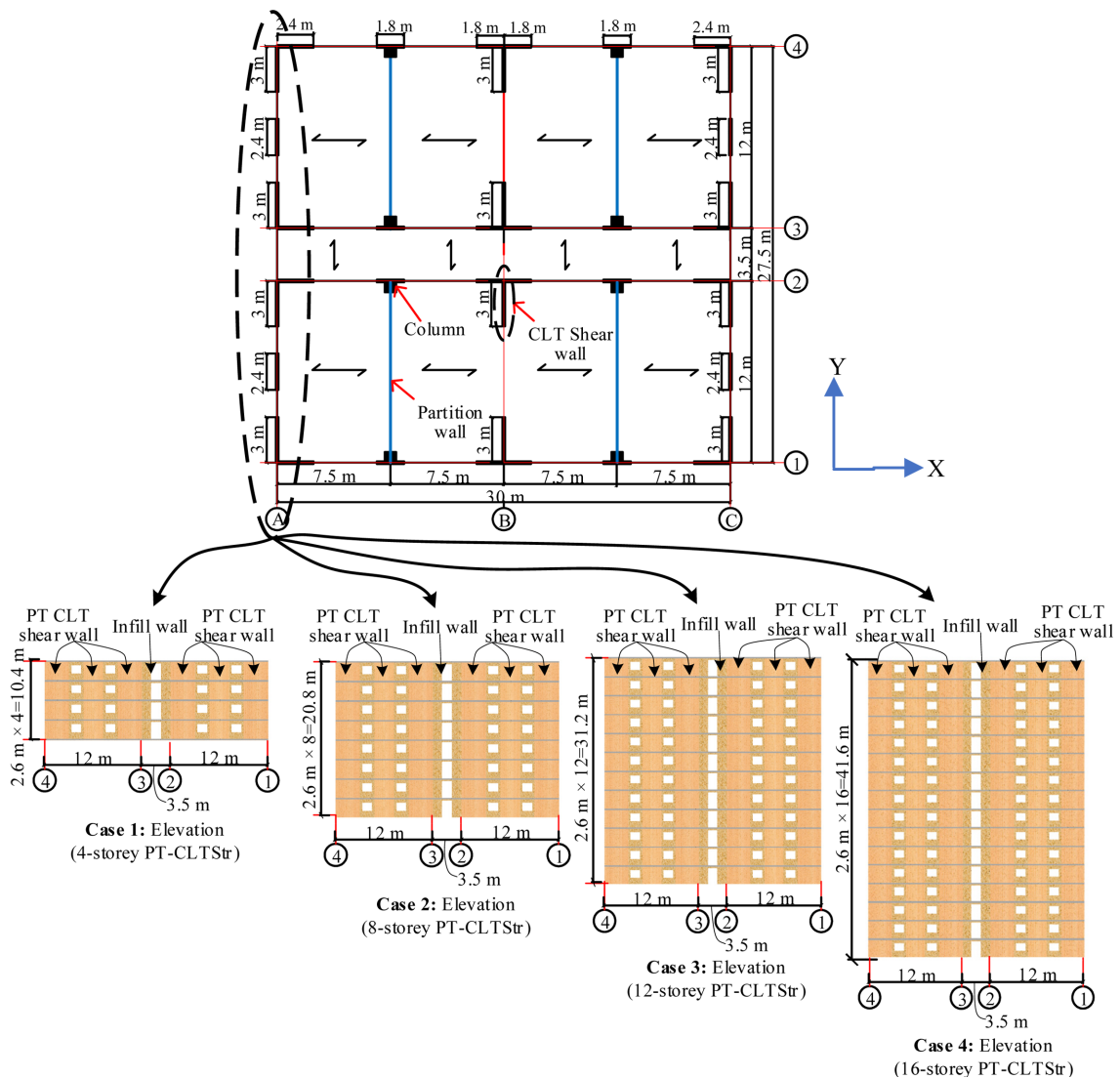
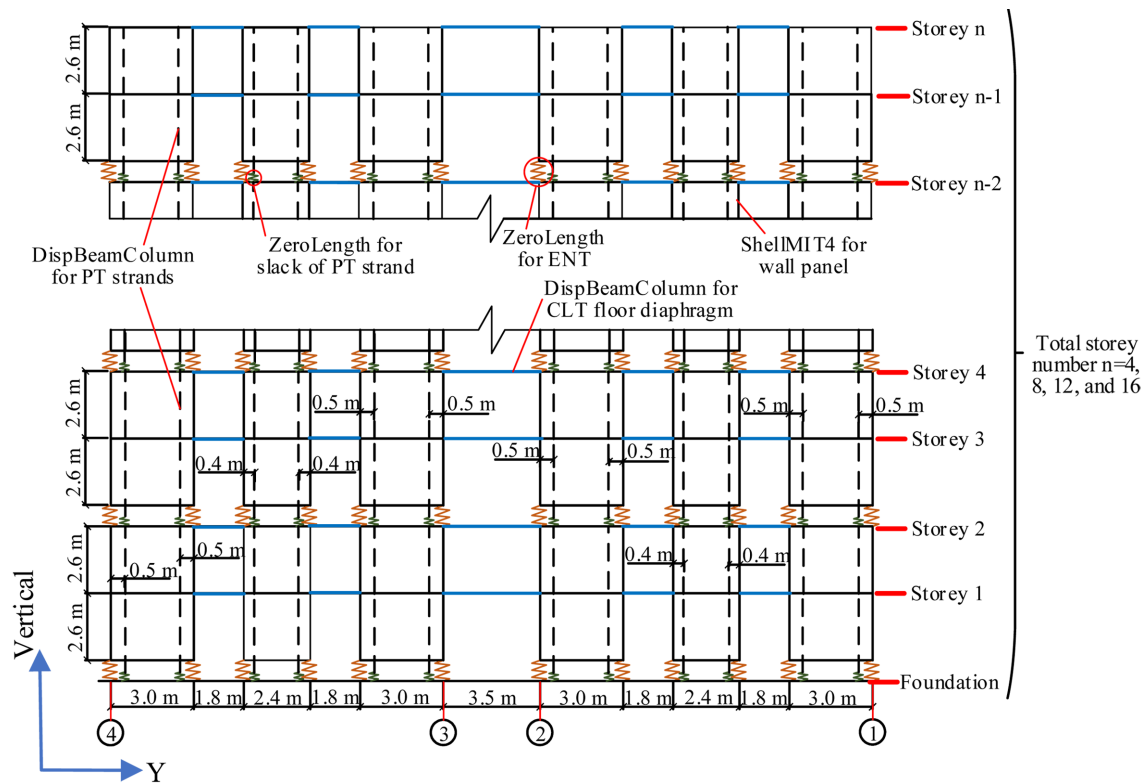


Figure 2. Floor Layout of the Benchmark PT CLT Shear Wall Structures.

Table 1. The Shear Wall Layout for the 4-storey PT-CLTstr (Y Direction)

Width	2.4 m		3.0 m		Resistance (kN)
Storey	No.	Configuration	No.	Configuration	
1-2	4	30.7 % initial PT stress ratio; 21.8-mm-diameter PT strand;	12	46.1 % initial PT stress ratio; 17.8-mm-diameter PT strand;	2586.4
3-4	4	30.7 % initial PT stress ratio; 17.8-mm-diameter PT strand;	12	30.7 % initial PT stress ratio; 15.2-mm-diameter PT strand;	1571.7

**Figure 3.** Simplified Two-dimensional sTstructural Model of PT-CLTstrs.

strands and for simulating the floor diaphragms that connect the neighboring PT CLT shear walls, respectively. The ShellMIT4 element combined with the J2Plasticity material law was used for simulating the CLT wall panels. The ZeroLength element combined with the ENT material law was used for simulating the contact stiffness of the interface between the wall panel and the foundation. Based on structural modal analysis, for the 4-, 8-, 12-, and 16-storey benchmark PT-CLTstrs, their fundamental period T_1 was 1.40 s, 1.97 s, 2.40 s, and 2.99 s, respectively.

For the model of each PT-CLTstr, a set of 20 ground motions (V_{30} was between 280–480 m/s) was selected from the Pacific Earthquake Engineering Research Center's Next Generation Attenuation (NGA) database. These 20 ground motions used as the excitations of the structural dynamic analysis should match the target seismic response spectrum corresponding to the defined performance level of the DDD procedure (i.e., CP hazard level) with the fundamental period T_1 . Then, nonlinear dynamic analysis was conducted on the model of each PT-CLTstr, using the

corresponding assemble of the 20 ground motions. The maximum inter-storey drift (MaxISDR) of each PT-CLTstr were obtained, forming a cumulative curve of MaxISDR based on the empirical cumulative distribution functions. Since the probability of non-exceedance (PNE) was defined as 95% based on the Chinese code GB 50068 (2018), the inter-storey drift limitation of the PT-CLTstrs for the CP hazard level can be determined in the range of 2.0%–2.4%, as shown in Figure 4. This drift range of 2.0%–2.4% is in agreement with the recommended drift limitation of 2.2% for the PT-CLTstrs under the CP hazard level (Sun *et al.* 2019 and 2020c), indicating that the models of the PT-CLTstrs were calibrated.

3. Fragility-based Reliability Analysis

3.1. General Introduction

In the fragility-based reliability analysis, fragility analysis was used for estimating the structural non-performance probability conditional on a given seismic hazard level

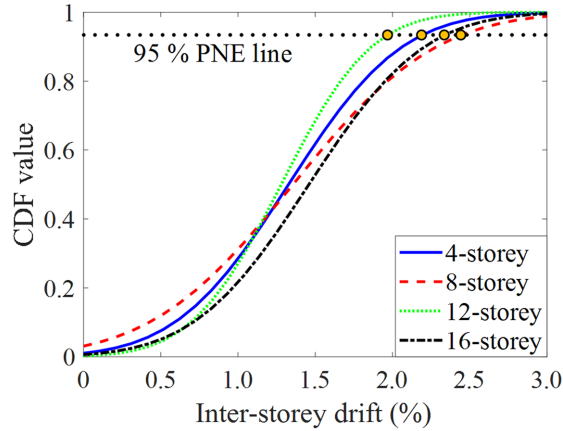


Figure 4. CDF Curves of the Structural Inter-storey Drift.

(e.g., IO, LS, CP). This conditional non-performance probability was then multiplied by the annual probability of exceeding a given seismic intensity measure (IM), producing a structural failure probability. Therefore, for one PT-CLTstr, its structural failure probability can be calculated using equation 1, in which, $f_R(z)$ is the probability density function of the seismic fragility; $H_{IM}(z)$ is the hazard function for earthquakes with a given IM . The discrete form of equation 1 can be expressed as equation 2, in which, the $F_R(IM_i)$ is the conditional non-performance probability (i.e., structural fragility) for the i -level IM ; $H_{IM}(IM_i)$ is the annual probability of exceeding the given i -level IM .

$$P_f = \int f_R(z) \cdot H_{IM}(z) \cdot dz \quad (1)$$

$$P_f = \sum [F_R(IM_i) - F_R(IM_{i-1})] \cdot H_{IM}(IM_i) \quad (2)$$

3.2. Fragility Analysis

The fragility analysis can be conducted using probability seismic demanding analysis (PSDA) or incremental dynamic analysis (IDA). Since it was proven that both PSDA and

IDA can generate similar fragility curves but the PSDA required less computational efforts (Zhang and Huo 2009), in this paper, the fragility analysis for estimating the conditional non-performance probability was conducted using the PSDA method; besides, the PGAs (peak ground accelerations) of the ground motions were recommended as the IM (Padgett *et al.* 2008). A total of 10 earthquake ground motions (V_{30} was between 280-480 m/s) were selected as the input excitations for PSDA (Table 2), including 6 shallow crustal ground motions from NGA database, 3 subduction ground motions from the Japanese database of the K-NET and KiK-net, and 1 Wenchuan (a city of Sichuan) ground motion. These selected ground motions with PGAs evenly distributed in the range of 0.1 g - 1.5 g can reflect the seismic environments of Sichuan, producing unbiased seismic performance evaluation on the PT-CLTstrs.

In this paper, the seismic reliability of each PT-CLTstr was calculated for three earthquake hazard levels, including the IO hazard level with an average return period of 50 years, the LS hazard level with an average return period of 475 years, and the CP hazard level with an average return period of 2475 years. The MaxISDR of the PT-CLTstrs was adopted as the engineering demanding parameter (EDP) for the PSDA; besides, the damage index of the MaxISDR (θ_{DI}) was adopted as 0.7%, 1.4%, and 2.2% for the IO, LS, and CP hazard levels, respectively (Sun *et al.* 2019). The fragility curves of the PT-CLTstrs providing their conditional non-performance probabilities are shown in Figure 5.

3.3. Seismic Hazard and Failure Probability

The annual probability of exceeding a given PGA [i.e., $H_{IM}(PGA)$] can be calculated using equation (3) (Cornell *et al.* 2002). For the IO with a 50-year return period, LS with a 475-year return period, and CP with a 2475-year return period, their mean PGA is recommended as 0.20 g, 0.55 g, and 0.82 g, respectively (Shu *et al.* 2019). The seismic hazard curve for annual exceedance probabilities was obtained (Figure 6) by fitting the mean PGA of each hazard level with its corresponding return period. The

Table 2. Ground Motions Selected for Reliability Analysis

No.	Event	Date	Station	Component	PGA (g)	Type
1	Chi-Chi, Taiwan	1999.9.20	TCU036	TCU036-N	0.124	Shallow
2	Irpinia, Italy-01	1980.11.23	Sturno (STN)	STU000	0.227	Shallow
3	Northridge-01	1994.1.17	Pardee-SCE	PAR-T	0.302	Shallow
4	Superstition Hills-02	1987.11.24	Parachute Test Site	PTS315	0.384	Shallow
5	Cape Mendocino	1992.4.15	Centerville Beach	CBF360	0.478	Shallow
6	Cape Mendocino	1992.4.15	Petrolia	PET090	0.662	Shallow
7	TOHKAMACHI	2004.10.23	NIG021	NS	0.832	Subduction
8	Kobe, Japan	1995.1.26	KJMA	KJM000	0.832	Subduction
9	Wenchuan	2008.5.12	Wolong	EW	0.977	Subduction
10	SHIOGAMA	2011.4.7	MYG012	EW	1.457	Subduction

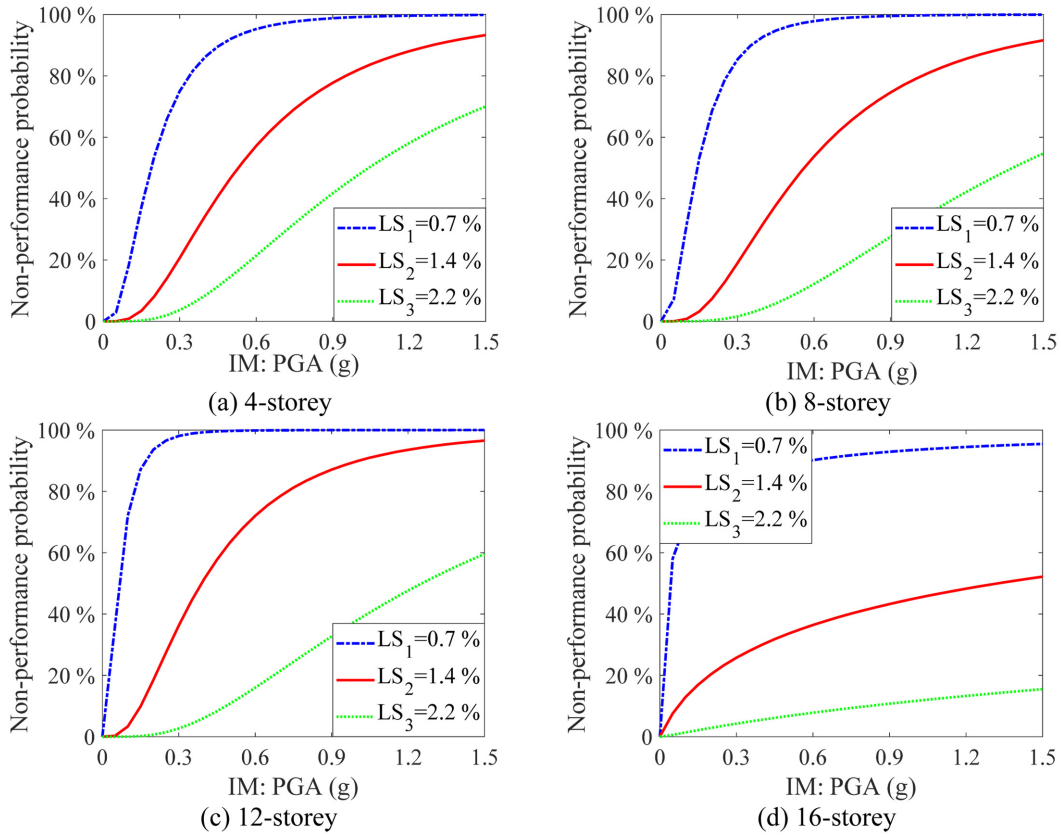


Figure 5. Fragility Curves of the PT-CLTstrs.

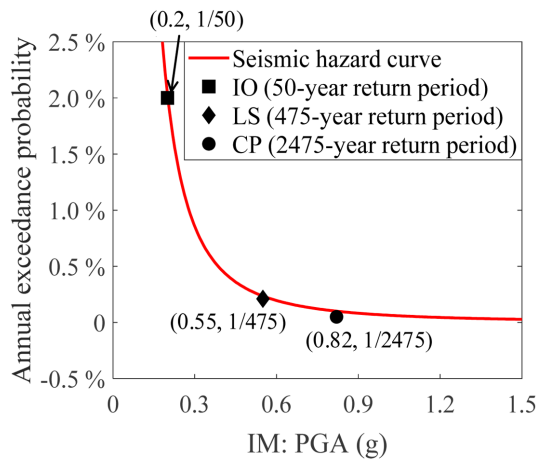


Figure 6. Seismic Hazard Curve for Annual Exceedance Probability.

regression analysis yielded a decay factor k_d of 2.131 and a scale factor of 0.000657. Then, the specific $H_{IM}(PGA)$ of the PT-CLTstrs can be calculated using the equation 3.

$$H_{IM}(PGA) = k_s \cdot (PGA)^{-k_d} \tag{3}$$

Based on the equation 2, product of both the $H_{IM}(PGA)$ and the structural fragility was integrated over a PGA range of 0.1 g - 1.5 g, producing a failure probability P_f and a corresponding reliability index β for each PT-CLTstr or for each seismic hazard level. Results of the fragility-based reliability analysis are listed in Table 3. For the IO hazard level, the β of the four PT-CLTstrs is in the range of 1.484 - 1.942, with the largest β for the 4-storey PT-CLT. For the LS hazard level, the β of the four PT-CLTstrs is in the range of 2.200 - 2.614, with the largest β for the 8-storey PT-CLT. For the CP hazard level, the β

Table 3. Fragility-based Reliability Analysis Results

Storey	IO		LS		CP	
	P_f	β	P_f	β	P_f	β
4	2.606×10^{-2}	1.942	4.793×10^{-3}	2.590	13.300×10^{-4}	3.005
8	3.732×10^{-2}	1.783	4.476×10^{-3}	2.614	7.833×10^{-4}	3.162
12	6.888×10^{-2}	1.484	8.976×10^{-3}	2.367	10.284×10^{-4}	3.082
16	6.431×10^{-2}	1.520	13.889×10^{-3}	2.200	18.213×10^{-4}	2.908

of the four PT-CLTstrs is in the range of 2.908 - 3.162, with the largest β for the 8-storey PT-CLT.

4. Reliability Based on Response Surface Method

4.1. General Introduction

Compared to the fragility-based reliability analysis method, the response surface method (RSM) can consider more random variables, which is always coupled with common reliability analysis methods [e.g., first-order reliability method (FORM)]. In the RSM for the PT-CLTstrs, the performance function that serves as an effective tool for reliability estimation or structural optimization can be expressed as equation 4, in which, δ is the inter-storey drift capacity of the PT-CLTstrs ($\delta = H \cdot \theta_{DI}$); Δ is the MaxISDR demand, which a function of the seismic intensity measure IM , the characteristics of the ground motions r , the structural total floor number n , the response surface fitting error ε , and the design factors of interest F_d . The characteristics of the ground motions r can be considered by selecting a set of representative ground motions reflecting the site record-to-record variability. The PGAs of the ground motions were used as the IM , which follow a lognormal distribution with a mean PGA of 0.25 g and with a COV (coefficient of variation) of 0.6 (Li *et al.* 2012); it coupled with an assumed annual Poisson arrival rate of 0.1/year. In this paper, the uncertainties including the IM (i.e., PGA), the total floor number n , and the fitting error ε were considered in the performance function of the PT-CLTstrs (equation 5).

$$G = \delta - \Delta(IM, r, n, \varepsilon, F_d) \quad (4)$$

$$G = \delta - \Delta(PGA, n, \varepsilon) \quad (5)$$

15 PGA levels (i.e., from 0.1 g to 1.5 g with intervals of 0.1 g) and 4 total floor number levels (i.e., 4-, 8-, 12-, and 16-storey) were used for generating the database of the MaxISDR. In this paper, the 10 ground motions listed in Table 2 were scaled with respect to each PGA level, generating 15 groups of ground motions with incremental PGA levels. For each PT-CLTstr, over a group of 10 ground motions scaled to one PGA level, the structural MaxISDR was calculated based on the time-history dynamic analysis. For each PT-CLTstr and for each PGA level, both the mean value (μ_{sm}) and the standard deviation (σ_{sm}) of the MaxISDR were calculated based on the structural model simulations; then, for all the combinations of the PGA levels and the floor number levels, a discrete set of the μ_{sm} or the σ_{sm} was generated (Table 4).

4.2. Response surface and failure probability

Since the uncertainties (i.e., random variables) including the PGA, the total floor number n , and the fitting error ε were considered in this paper, the polynomial functions (equations 6-7) were respectively used to fit the set of the μ_{sm} and to fit the set of the σ_{sm} s over the domain of the considered random variables; in which, the μ_{rs} and the σ_{rs} are respectively the mean value and the standard deviation of the MaxISDR calculated using the polynomial fitting functions (i.e., results from response surfaces). a_{ij} and b_{ij} are the coefficients estimated by minimizing the square

Table 4. Statistical data of the structural simulation results (μ_{sm} and σ_{sm})

PGA (g)	Structural total floor number n							
	4		8		12		16	
	μ_{sm} (mm)	σ_{sm} (mm)	μ_{sm} (mm)	σ_{sm} (mm)	μ_{sm} (mm)	σ_{sm} (mm)	μ_{sm} (mm)	σ_{sm} (mm)
0.1	4.248	0.961	7.860	3.292	9.268	5.029	7.505	4.189
0.2	14.647	11.959	15.404	6.233	18.325	9.906	14.832	8.294
0.3	16.818	6.371	23.013	9.389	27.225	14.428	22.288	12.551
0.4	35.092	24.338	30.149	11.797	35.728	18.530	29.456	16.380
0.5	28.281	15.244	36.548	14.444	44.308	22.542	36.595	20.171
0.6	57.101	45.413	43.605	16.273	53.002	26.442	43.647	23.631
0.7	44.711	24.906	50.806	19.171	61.131	30.463	50.811	27.116
0.8	48.845	21.817	57.790	20.744	69.488	34.295	57.700	31.483
0.9	50.675	19.396	64.892	23.914	77.441	37.807	64.827	35.361
1.0	70.001	31.453	71.206	26.615	85.608	40.889	72.195	38.809
1.1	59.505	26.451	77.985	29.281	93.944	44.827	79.206	43.301
1.2	67.848	26.463	85.779	32.202	102.049	48.536	86.455	47.398
1.3	59.569	18.897	91.926	34.381	109.822	52.063	92.449	50.610
1.4	65.672	23.871	97.742	36.665	117.817	55.479	99.041	54.090
1.5	76.541	20.215	105.824	34.702	125.358	58.613	105.728	57.696

error between the polynomial fitting results and the model simulation results; superscripts i, j , and k are the orders of the polynomials. In this paper, third-order polynomials with nine coefficients were adopted (i.e., i and $j=1, 2, 3$) in the polynomial functions (equations 8-9).

$$\mu_{rs} = \sum a_{ij} \cdot PGA^i \cdot n^j \quad (6)$$

$$\sigma_{rs} = \sum a_{ij} \cdot PGA^i \cdot n^j \quad (7)$$

$$\begin{aligned} \mu_{rs} = & a_{11} \times PGA \cdot n + a_{12} \times PGA \cdot n^2 + a_{21} \times PGA^2 \cdot n + a_{22} \\ & \times PGA^2 \cdot n^2 + a_{13} \times PGA \cdot n^3 + a_{31} \times PGA^3 \cdot n + a_{23} \\ & \times PGA \cdot n + a_{32} \times PGA^3 \cdot n^2 + a_{33} \times PGA^3 \cdot n^3 \end{aligned} \quad (8)$$

$$\begin{aligned} \sigma_{rs} = & b_{11} \times PGA \cdot n + b_{12} \times PGA \cdot n^2 + b_{21} \times PGA^2 \cdot n + b_{22} \\ & \times PGA^2 \cdot n^2 + b_{13} \times PGA \cdot n^3 + b_{31} \times PGA^3 \cdot n + b_{23} \\ & \times PGA \cdot n + b_{32} \times PGA^3 \cdot n^2 + b_{33} \times PGA^3 \cdot n^3 \end{aligned} \quad (9)$$

When taking the fitting error ε into account, the fitting errors of the generic i -th combination of the random variables were calculated using equations 10-11. The mean and standard deviation of the overall fitting errors (i.e., ε_μ and ε_σ) can be obtained when all the combinations

are considered, both of which are assumed to follow a normal distribution. Assuming that the seismic response of MaxISDR follows a lognormal distribution, the performance function (i.e., equation 5) can be rewritten as equation 12, in which, μ is the mean value of MaxISDR demand calculated using equation 13; V is the COV (i.e., σ/μ), σ is the standard deviation of MaxISDR demand calculated using equation 14. R_N is the standard normal distribution $R_N(0, 1)$.

$$\varepsilon_\mu^i = \frac{\mu_{rs}^i - \mu_{sm}^i}{\mu_{rs}^i} \quad (10)$$

$$\varepsilon_\sigma^i = \frac{\sigma_{rs}^i - \sigma_{sm}^i}{\sigma_{rs}^i} \quad (11)$$

$$G = \delta - \frac{\mu}{\sqrt{1+V^2}} \exp(R_N \sqrt{\ln(1+V^2)}) \quad (12)$$

$$\mu = \mu_{rs} \cdot (1 - \varepsilon_\mu) \quad (13)$$

$$\sigma = \sigma_{rs} \cdot (1 - \varepsilon_\sigma) \quad (14)$$

The polynomial response surfaces for both the mean

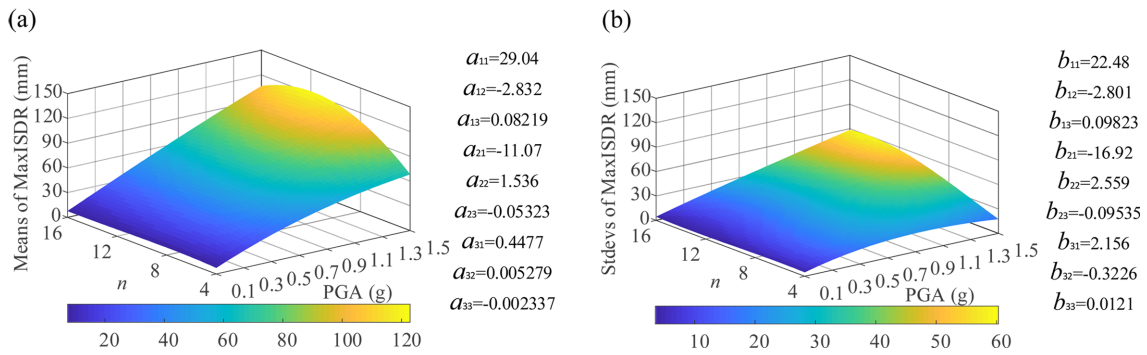


Figure 7. Polynomial Response Surfaces: (a) Mean Values; (b) Standard Deviations.

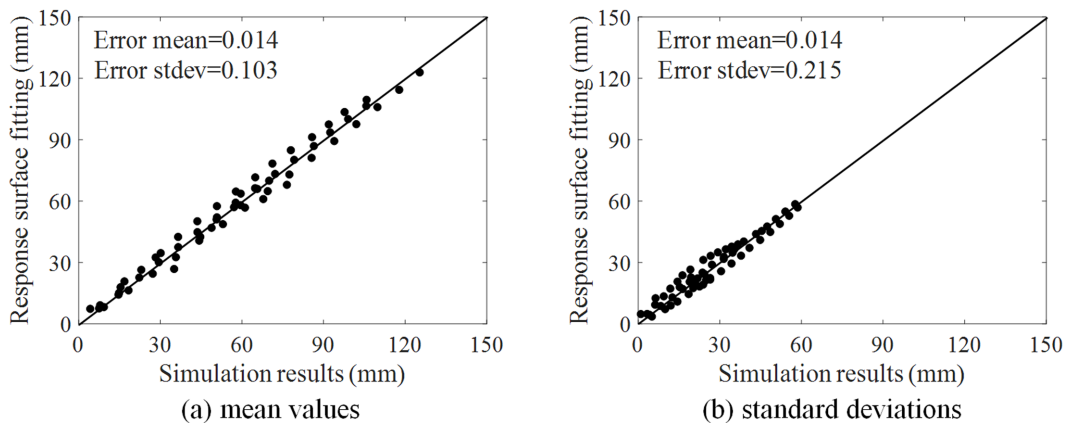


Figure 8. Polynomial Response Surface Fitting Results Versus Simulation Results.

Table 5. RSM-based Reliability Analysis Results

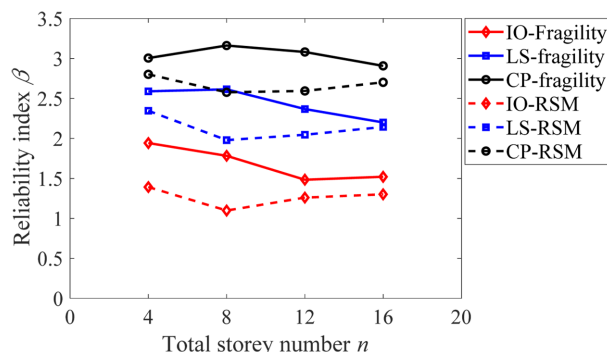
Storey	IO		LS		CP	
	P_f	β	P_f	β	P_f	β
4	8.200×10^{-2}	1.392	9.484×10^{-3}	2.346	2.501×10^{-3}	2.802
8	13.606×10^{-2}	1.098	23.931×10^{-3}	1.979	4.982×10^{-3}	2.577
12	11.383×10^{-2}	1.260	20.372×10^{-3}	2.046	4.746×10^{-3}	2.594
16	9.661×10^{-2}	1.301	16.023×10^{-3}	2.144	3.447×10^{-3}	2.702

values and the standard deviations of the MaxISDR are shown in Figure 7; the nine fitted polynomial coefficients are also listed for each polynomial response surface. The polynomial fitting errors for the sets of both the μ_{sm} and the σ_{sm} are shown in Figure 8. Most of the data points are located near the perfect agreement line, indicating that good fitting results with small fitting errors can be achieved by using the third-order polynomial response surfaces.

Then, the structural failure probability P_f and the reliability index β can be estimated based on the FORM using the software of *Rt* (Mahsuli and Haukaas 2013). The RSM-based reliability analysis results with respect to both the 15 PGA levels and the 4 total floor number levels are listed in Table 5. For the IO hazard level, the β of the four PT-CLTstrs is in the range of 1.098 - 1.392. For the LS hazard level, the β of the four PT-CLTstrs is in the range of 1.979 - 2.346. For the CP hazard level, the β of the four PT-CLTstrs is in the range of 2.577 - 2.802. The largest β is for the 4-storey PT-CLTstr under all seismic hazard levels.

5. Comparison and Discussion

The seismic reliability of the PT-CLTstrs under different seismic hazard levels was evaluated, based on the fragility analysis combined with the seismic hazard analysis as well as based on the RSM combined with the FORM, respectively. The reliability indices of the PT-CLTstrs are shown in Figure 9. The RSM-based reliabilities of the PT-CLTstrs that consider more intervening random variables (i.e., the response surface fitting error, the total storey

**Figure 9.** Reliability Indices of the PT-CLTstrs.

number, and the earthquake ground motions) are slightly less than the fragility-based reliabilities. Overall, the reliability method based on the fragility analysis and that based on the response surface can provide similar reliability indices; For these studied 4-, 8-, 12-, and 16-storey PT-CLTstrs, following their fragility-based reliabilities, the 8-storey PT-CLTstr with the largest β under the LS and CP hazard levels is subjected to the least seismic vulnerability; while, following their RSM-based reliabilities, the 4-storey PT-CLTstr with the largest β under all hazard levels is subjected to the least seismic vulnerability.

When a random variable (e.g., the ground motions) is the dominant reliability-influencing one, then the fragility-based reliability analysis method seems to be more straightforward for obtaining the structural seismic reliabilities. Because compared to the fully coupled reliability analysis method (i.e., RSM), the fragility-based reliability analysis method separates the structural response analysis from the seismic hazard analysis. Overall, both methods can be used as efficient approaches for assessing the seismic reliabilities of the PT-CLTstrs.

6. Conclusions

In this paper, seismic reliability assessment was conducted on a set of mid- and high-rise PT-CLTstrs designed with the direct displacement-based seismic design method, based on the fragility analysis combined with the seismic hazard analysis as well as based on the RSM combined with the FORM, respectively. The main conclusions can be drawn as follows:

1. Based on the fragility-based reliability analysis method, the reliability indices of the PT-CLTstrs are in the range of 1.484 - 1.942, 2.200 - 2.614, and 2.908 - 3.162, for the IO, LS and CP hazard levels, respectively.
2. Based on the RSM-based reliability analysis method, the reliability indices of the PT-CLTstrs are in the range of 1.098 - 1.392, 1.979 - 2.346, and 2.577 - 2.802, for the IO, LS and CP hazard levels, respectively.
3. The RSM-based reliabilities considering more random variables are slightly less than the fragility-based reliabilities. Overall, both the RSM and the fragility-based reliability method can be used as efficient approaches for assessing the seismic reliabilities of the PT-CLTstrs.
4. For these studied 4-, 8-, 12-, and 16-storey PT-CLTstrs, following their fragility-based reliabilities, overall, the 8-

storey PT-CLTstr is subjected to the least seismic vulnerability; while, following their RSM-based reliabilities, the 4-storey PT-CLTstr is subjected to the least seismic vulnerability.

Acknowledgements

The authors also gratefully acknowledge the support from National Natural Science Foundation of China (Grant NO. 51778460) and China Scholarship Council (Grant NO. 201706260124). Ground motion data for Japanese earthquakes and worldwide crustal earthquakes were obtained from the K-NET/KiK-net database at <http://www.kyoshin.bosai.go.jp/>, and the PEER-NGA database at <http://peer.berkeley.edu/nga/index.html>, respectively.

References

- Akbas, T., Sause, R., Ricles, J. M., Ganey, R., Berman, J., Loftus, S., Daniel, J. D., Pei, S. L., van de Lindt, J., Blomgren, H. E. (2017). "Analytical and experimental lateral-load response of self-centering post-tensioned CLT walls." *J. Struct. Eng.*, 143(6), 04017019.
- Blomgren, H. E., Pei, S., Jin, Z., Powers, J., Dolan, J. D., van de Lindt, J. W. (2019). "Full-scale shake table testing of cross-laminated timber rocking shear walls with replaceable components." *J. Struct. Eng.*, 145(10), 04019115.
- Buchanan, A., Iqbal, A., Palermo, A. G., Pampanin, S. (2007). "Improved seismic performance of LVL post-tensioned walls coupled with UFP devices." In: 8th Pacific conf. On earthquake engineering. New Zealand Society for Earthquake Engineering and Nanyang Technological Univ., School of Civil and Environmental Engineering, Wellington, New Zealand, 1-9.
- Ceccotti, A., Sandhaas, C., Okabe, M., Yasumura, M., Minowa, C., Kawai, N. (2013). "SOFIE project- 3D shaking table test on a seven-storey full-scale cross-laminated building." *Earthq. Eng. Struct. Dyn.*, 42(13), 2003-2021.
- Chen, Z., Popovski, M., Iqbal, A. (2020). "Structural performance of post-tensioned CLT shear walls with energy dissipaters." *J. Struct. Eng.*, 146(4), 04020035.
- Cornell, C. A., Jalayer, F., Hamburger, R. O., Foutch, D. A. (2002). "Probabilistic basis for 2000 SAC federal emergency management agency steel moment frame guidelines." *J. Struct. Eng.*, 128(4), 526-533.
- Deng, P., Pei, S., van de Lindt, J., John, W., Omar Amini, M., Liu, H. (2019). "Lateral behavior of panelized CLT walls: A pushover analysis based on minimal resistance assumption." *Eng. Struct.*, 191, 469-478.
- Ganey, R., Berman, J., Akbas, T., Loftus, S., Daniel Dolan, J., Sause, R., Ricles, J., Pei, S. L., van de Lindt, J., Blomgren, H. E. (2017). "Experimental investigation of self-centering crosslaminated timber walls." *J. Struct. Eng.*, 143(10), 04017135.
- Gavric, I., Fragiaco, M., Ceccotti, A. (2015). "Cyclic behavior of CLT wall systems: experimental tests and analytical prediction models." *J. Struct. Eng.*, 141(11), 04015034.
- He, M. J., Sun, X. F., Li, Z. (2018). "Bending and compressive properties of cross-laminated timber (CLT) panels made from Canadian hemlock." *Constr. Build. Mater.*, 185, 175-183.
- Hong, H. P., Yang, S. C. (2019). "Reliability and fragility assessment of the mid-and high-rise wood buildings subjected to bidirectional seismic excitation." *Eng. Struct.*, 201, 109734.
- Li, M., Lam, F., Foschi, R. O., Nakajima, S., Nakagawa, T. (2012). "Seismic performance of post-and-beam timber buildings II: reliability evaluations." *J. Wood. Sci.*, 58(2), 135-143.
- Mahsuli, M., Haukaas, T. (2013). "Computer program for multi-model reliability and optimization analysis." *J. Comput. Civil. Eng.*, 27(1), 87-98.
- GB 50068 (2018). *Unified standard for reliability design of building structures*. Ministry of Construction of the People's Republic of China. Beijing, China. (in Chinese).
- Newcombe, M. P., Pampanin, S., Buchanan, A. H. (2010). "Design, fabrication and assembly of a two-storey post-tensioned timber building." In: Proc. World Conference on Timber Engineering, Trentino, Italy, 3092-3100.
- Padgett, J. E., Nielson, B. G., DesRoches, R. (2008). "Selection of optimal intensity measures in probabilistic seismic demand models of highway bridge portfolios." *Earthq. Eng. Struct. Dyn.*, 37(5), 711-725.
- Pai, S. G. S., Lam, F., Haukaas, T. (2017). "Force Transfer around openings in Cross-laminated timber shear walls." *J. Struct. Eng.*, 143(4), 4016215.
- Palermo, A., Pampanin, S., Buchanan, A. (2006). "Experimental investigations on LVL seismic resistant wall and frame subassemblies." In: Proc. Of first European conference on earthquake engineering and seismology, Geneva, Switzerland, No. 983.
- Pei, S., van de Lindt, J. W., Barbosa, A. R., Berman, J. W., McDonnell, E., Daniel Dolan, J., et al. (2019). "Experimental seismic response of a resilient 2-story mass-timber building with post-tensioned rocking walls." *J. Struct. Eng.*, 145(11), 04019120.
- Porcu, M. C., Bosu, C., Gavrić, I. (2018). "Non-linear dynamic analysis to assess the seismic performance of cross-laminated timber structures." *J. Build. Eng.*, 19, 480-493.
- Sarti, F., Palermo, A., Pampanin, S., Berman, J. (2017). "Determination of the seismic performance factors for post-tensioned rocking timber wall systems: seismic performance factors for post-tensioned timber wall systems." *Earthq. Eng. Struct. Dyn.*, 46, 181-200.
- Sarti, F., Palermo, A., Pampanin, S. (2015). "Quasi-static cyclic testing of two-thirds scale un-bonded post-tensioned rocking dissipative timber walls." *J. Struct. Eng.*, 142(4), E4015005.
- Shahnewaz, M., Popovski, M., Tannert, T. (2019). "Resistance of cross-laminated timber shear walls for platform-type construction." *J. Struct. Eng.*, 145(12), 4019149.
- Shu, Z., Li, S., Sun, X. F., He, M. J. (2019). "Performance-based seismic design of pendulum tuned mass damper system." *J. Earthq. Eng.*, 23(2), 334-355.
- Smith, T., Ludwig, F., Pampanin, S., Fragiaco, M., Buchanan, A., Deam, B., Palermo, A. (2007). "Seismic response of hybrid-LVL coupled walls under quasi-static and pseudodynamic testing." In: Proc. Of New Zealand society for earthquake engineering conference, Palmerston

- North, New Zealand, Vol. 8.
- Stellacci, S., Rato, V., Poletti, E., et al. (2018). "Multi-criteria analysis of rehabilitation techniques for traditional timber frame walls in Pombalino buildings (Lisbon)." *J. Build. Eng.*, 16, 184-198.
- Sun, X. F., He, M. J., Li, Z., Lam, F. (2019). "Seismic performance assessment of conventional CLT shear wall structures and post-tensioned CLT shear wall structures." *Eng. Struct.*, 196, 109285.
- Sun, X. F., He, M. J., Li, Z. (2020a). "Experimental and analytical lateral performance of post-tensioned CLT shear walls and conventional CLT shear walls." *J. Struct. Eng.*, DOI: 10.1061/(ASCE)ST.1943-541X.0002638.
- Sun, X. F., He, M. J., Li, Z., Lam, F. (2020b). "Seismic performance of energy-dissipating post-tensioned CLT shear wall structures I: Shear wall modeling and design procedure." *Soil. Dyn. Earthq. Eng.*, 131, 106022.
- Sun, X. F., He, M. J., Li, Z., Lam, F. (2020c). "Seismic performance of energy-dissipating post-tensioned CLT shear wall structures II: Dynamic analysis and dissipater comparison." *Soil. Dyn. Earthq. Eng.*, 130, 105980.
- van de Lindt, J. W., Walz, M. A. (2003). "Development and application of wood shear wall reliability model." *J. Struct. Eng.*, 129(3), 405-413.
- van de Lindt, J. W., John, W., Furley, J., Amini, M. O., Pei, S., Tamagnone, G., Barbosa, A. R., et al. (2019). "Experimental seismic behavior of a two-story CLT platform building." *Eng. Struct.*, 183, 408-422.
- Wilson, A. W., Motter, C. J., Phillips, A. R., Dolan, J. D. (2019). "Modeling techniques for post-tensioned cross-laminated timber rocking walls." *Eng. Struct.*, 195, 299-308.
- Zhang, J., Huo, Y. L. (2009). "Evaluating effectiveness and optimum design of isolation devices for highway bridges using the fragility function method." *Eng. Struct.*, 31(8), 1648-1660.
- Zhang, X., Shahnewaz, M., Tannert, T. (2018). "Seismic reliability analysis of a timber steel hybrid system." *Eng. Struct.*, 167: 629-638.